EUROPEAN ORGANIZATION FOR NUCLEAR RESEARCH

L3 Internal Note 1800
July 7, 1995

Search for Neutral Higgs bosons production through the process $Z \to Z^* H^0$

The L3 Collaboration

Abstract

We report on the searches for the neutral Standard Model Higgs boson production, in the process $e^+e^- \to Z^* H^0$, performed with data collected by L3 detector from 1991 to 1994, equivalent to about 3.05 M hadronic decays of the Z, at LEP e^+e^-collider. Three decay channels of the Z have been taken into account: $H^0 e^+ e^-$, $H^0 \mu^+ \mu^-$, $H^0 \nu \bar{\nu}$. We searched for the production of a Higgs boson with a mass below 70 GeV and we did not find any evidence of the signal in all the mass range. Therefore we can set a 95 % C.L. lower limit on the mass of the Standard Model Higgs boson of 60.2 GeV . These searches can also be considered in the framework of the general two doublet model and limits on the Higgs bosons production through the process $e^+e^- \to Z^* h^0$ are set also assuming invisible decays of the Higgs boson. For the latter case we derived a 95 % C.L. lower limit on the mass of the Higgs boson of 66.7 GeV for a production cross section equal to that of the Standard Model.

Sumbitted to the EPS and Lepton-Photon Conferences, July 1995

Introduction

The Minimal Standard Model [1] predicts the existence of a neutral scalar Higgs particle H^0 [2]. In the framework of this model the couplings of the H^0 boson to the fermions and to the gauge vector bosons are known but its mass is not specified.

The main production mechanism of the Higgs boson at LEP is predicted to be through the decay of the Z boson into an H^0 and a virtual Z^* [3]

$$e^+e^- \to Z \to H^0 + Z^* \to H^0 + f\bar{f}.$$

A heavy Higgs boson (with mass exceeding 11 GeV) decays predominantly into a $b\bar{b}$ pair, although the branching ratios into $c\bar{c}$ and $\tau^+\tau^-$ are not negligible.

Latest theoretical calculations [4, 5] of full one loop radiative corrections for the Standard Model Higgs production and decay are used and the branching ratio into $\tau^+\tau^-$ for a 60 GeV Higgs boson is set to 9.0%.

In two doublet models, where five scalar physical Higgs bosons are predicted (two charged H^+,H^-, two neutral CP even H^0,h^0 and one neutral CP odd A^0 ,) the bremsstrahlung process:

$$e^+e^- \to Z^*h^0$$

is still possible, where h^0 is the lightest neutral CP even Higgs, but one has to take into account a model dependent factor which reduces the production rate. In the Minimal Supersymmetric Standard Model (MSSM) this factor is equal to $\sin^2(\beta-\alpha)$ where α is the mixing parameter in the CP even Higgs sector while $\tan\beta$ is the ratio between the v.e.v. of the two Higgs doublets.

In addition to that we considered the possibility that h^0 decays in a pair of A^0 when kinematically allowed and also the possibility of invisible decay of the h^0 , which, for instance, is possible in R parity conserving supersymmetric models where h^0 may decay in a pair of χ (the lightest neutralino).

We report here on updated results of the search for bremsstrahlung production of the Higgs boson in the Minimal Standard Model and in general Two Doublet Models, in the mass range below to 70 GeV, in the channels $H^0\nu\bar{\nu}$, $H^0e^+e^-$ and $H^0\mu^+\mu^-$. We also report on the search for invisible Higgs decays never performed before by L3.

1 The L3 Detector

The L3 detector consists of a central tracking chamber (TEC), a high resolution electromagnetic calorimeter composed of BGO crystals, a ring of scintillation counters, a uranium and brass hadron calorimeter with proportional wire chamber readout, and an accurate muon chamber system. These detectors are installed in a 12 m diameter magnet which provides a uniform field of 0.5 T along the beam direction. Luminosity is measured with forward BGO arrays on each side of the detector. Low angle electrons are tagged by the active lead ring (ALR), a detector installed since 1992 which consists of lead planes alternated with scintillating material. A detailed description of each detector subsystem and its performance is given in Reference [6, 7].

2 Data Sample and Simulation

In these analyses we used 3.05 millions hadronic Z decay events, corresponding to approximately 117 pb^{-1} of integrated luminosity collected by L3 in the period 1991÷1994. In the analysis we considered only events for which both the hadronic and electromagnetic calorimeters, in addition to the muon chambers and the data acquisition system, were fully operational.

Monte Carlo events for the main background sources were generated.

- For $\mathrm{H}^0\nu\bar{\nu}$ channel we used:

  5.1 M $Z \rightarrow q\bar{q}$ generated using JETSET [8], 1.2 M $Z \rightarrow q\bar{q}$ generated using HERWIG [9], 0.2 M $Z \rightarrow b\bar{b} \rightarrow l\,\nu$ X generated using JETSET [8], 0.42 M $\gamma\gamma \rightarrow e^+e^-q\bar{q}$ generated using DIAG36, corresponding to approximately 75 pb^{-1}, 0.62 M $\gamma\gamma \rightarrow e^+e^-q\bar{q}$ and 0.05 M of $\gamma\gamma \rightarrow e^+e^-e^+e^-$ and $\gamma\gamma \rightarrow e^+e^-\mu^+\mu^-$ generated using VERMASEREN, 0.29 M $Z \rightarrow \tau^+\tau^-$ generated using KORALZ [10], 0.89 M bhabha events generated using BHAGENE3, and finally 500 events for each possible final state for the four fermion process generated using FERMSV [11] .

  Signal events were generated with the HIGGSMOD program for masses of the Higgs boson ranging from 2 to 70 GeV and with PYTHIA for masses below 2 GeV .

- For $\mathrm{H}^0e^+e^-$channel we used:

  2.5 M $Z \rightarrow q\bar{q}$ generated using JETSET [8], a number of $Z \rightarrow b\bar{b} \rightarrow e^+e^-X$ equivalent to about 7 M of hadronic decays generated using JETSET [8], 30 k bhabha events generated using BHAGENE3, 0.2 M $Z \rightarrow \tau^+\tau^-$ generated using KORALZ [10], 5500 events for the four fermion process $e^+e^-l\bar{l}$ and 27 k events for the four fermion process $e^+e^-q\bar{q}$. For the signal we generated events for each mass point from 10 MeV to 70 GeV using HIGGSMOD.

- For $\mathrm{H}^0\mu^+\mu^-$channel we used:

  2.29 M $Z \rightarrow q\bar{q}$ generated using JETSET [8], 0.22 M $Z \rightarrow b\bar{b} \rightarrow \mu\,\nu$ X (equivalent to about 4.8 M of hadronic decays) generated using JETSET [8], 5000 events for the four fermion process $\mu^+\mu^-q\bar{q}$ and 1000 events for the four fermion process $\mu^+\mu^-e^+e^-$ generated with `FERMISV` [11]. For the signal we have events for each Higgs mass value from 2 GeV up to 70 GeV generated with HIGGSMOD.

The detector response was fully simulated and additional time dependent detector inefficiencies were taken into account.

3 $\mathrm{H}^0\nu\bar{\nu}$ Channel

3.1 Detector Calibration and Event Reconstruction

Hadronic events were reconstructed using information coming from calorimeters, TEC and muon chambers. Energy clusters in the calorimeters are required to exceed a minimum energy threshold in order to be included in the event reconstruction. We also apply some quality cuts on tracks which are used in the analysis (minimum of 15 hits in the TEC, DCA less than 10 mm and a transverse momentum greater than 0.1 GeV). The energy of the event was obtained adding up the energy deposition in calorimeters with the momentum measured by TEC and muon chambers. We have calibration constants for different subdetectors of L3 and also for different regions of those subdetectors. In addition we have different calibration constants for matched and unmatched clusters and tracks. The effect of double counting of tracks and clusters is properly taken into account by weighting the calibration constants with the subdetector resolution to which they refer. With this new calibration we have observed a big improvement in energy resolution and also in jet direction resolution. Figure 1 shows the angular resolution on the directions of the jets for events which satisfy $q\bar{q}$ selection.

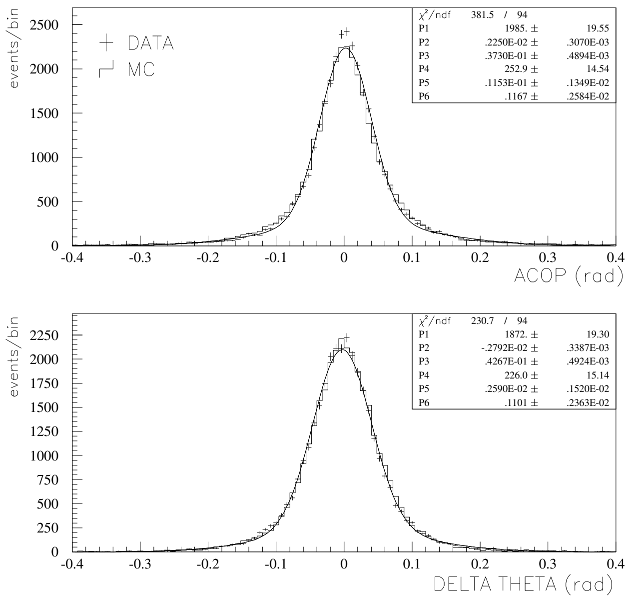

Figure 1: Distributions for the acoplanarity angle (top) between the two reconstructed jets and the polar angle difference (bottom) for the same jets, for data and Monte Carlo; the curves are the result of the fits of two gaussians to the data; the results of the fits are shown in the figure.

Events were reconstructed dividing the space into two hemispheres separated by a plane perpendicular to the thrust axis and forming a jet in each hemisphere. In addition to some natural variables such as the acoplanarity and acollinearity between the two jets we have defined some variables specific to this search: energy deposition in a cone of 25° h.o.a. around the missing energy direction in space (EM25) and in the same cone projected on the plane transverse to the beam line (EMF25); energy deposition in a cone of 60° h.o.a. around the vector opposite to the sum of the two jet directions in space (EC60); the sum of the angles in space between jets forcing the event reconstruction, performed in this case with the algorithm LUCLUS, to three jets (SJET); the ratio between the sum of particle momenta transverse to the jet direction and the jet energy ($\frac{\sum P_\perp}{E_{jet}}$), for the narrow jet (NOVN) and the broad jet (NOVB), where the broad jet is by definition the one with the biggest ratio $\frac{\sum P_\perp}{E_{jet}}$. The background rejection power of all these variables will be explained in the section dedicated to the selection procedure.

3.2 Mass Range 50 GeV $< M_H <$ 70 GeV

3.2.1 Study of Physical and Instrumental Backgrounds

The main signature of the neutrino decay channel is the presence of missing energy and two jets which are not back to back. These characteristics become less evident with increasing Higgs mass. So for a 60 GeV Higgs, the target of our analysis, the event signature is often present in

b decays of the Z and in $q\bar{q}\gamma$ events with the photon escaping detection. In order to optimize the choice of the variables and the rejection of our backgrounds a Monte Carlo study, at the generator level, has been performed.
As it is rather easy to reject $\tau^+\tau^-$ and $\gamma\gamma$ backgrounds we concentrated on $q\bar{q}$ events. We have reduced of a factor $2 * 10^5$ the $q\bar{q}$ Monte Carlo sample using a selection similar to the final one but with looser cuts. Among events selected in this way b decays of the Z^0 account for 50% of the sample and they have the following features: energy carried by neutrinos often greater than 5 GeV, $P_\perp$ of neutrino with respect to the b quark often greater than 1 GeV, and they also have a lot of energy lost in the beam pipe (often hard initial state photon). Other hadronic decays of the Z^0 are "dangerous" for different reasons. Actually they become "dangerous" because they are badly measured, in fact most of them have more than 10 GeV carried by neutral long lived hadrons. Furthermore most of them, due to fluctuations in the hadronization process, are very spherical events.
From this study we derived a selection, to be implemented at the generator level, which allows to simulate only 2% of $q\bar{q}$ events but including approximately 50% of most "dangerous" events. In addition to that we have a selection for events considered "dangerous" because they present photons escaping through dead BGO regions. With these selections we will produce a Monte Carlo sample equivalent to tens of millions hadronic Z^0 decays useful to test the analysis.

As important as physical background is instrumental background: with that we mean inefficiencies of the apparatus that are most important for our search. From this point of view an important source of background, which requires a detailed study, is $q\bar{q}\gamma$ topology when the photon escapes detection because of dead zones of the electromagnetic calorimeter. First of all we detected the regions of that calorimeter which were not working in the different data taking periods (from 1991 to 1994), studying the angular distribution of electromagnetic bumps in the calorimeter. Then we studied $q\bar{q}\gamma$ events as the following: the electromagnetic bump recognized as the photon is removed from the event reconstruction as it would happen for a photon going into a dead BGO zone. We apply a preliminary $H\nu\bar{\nu}$ selection to all $q\bar{q}\gamma$ events found in the data to estimate how important is this problem of dead BGO regions. Using the angular distribution of photons belonging to events survived to that selection and taking into account the luminosity weighted presence of dead zones (0.38% of the barrel region, corresponding to 0.28% of the total solid angle and 4.1% of the endcaps region, corresponding to 0.91% of the total solid angle) we estimate that the number of $q\bar{q}\gamma$ events for which the photon hits a dead BGO zone, so surviving to the Higgs selection at this stage, is approximately 7.

Furthermore $q\bar{q}\gamma$ events, reconstructed as previously explained, can be used to obtain the resolution for Higgs mass and missing energy direction. We took those events and we compared the reconstructed missing mass and missing momentum direction to the ones of the photon not included in the reconstruction.

Figure 2 shows data - Monte Carlo comparison for spatial missing momentum direction resolution, missing mass resolution, energy distribution and angular distribution of the radiated photon, after we have applied a preliminary $H^0\nu\bar{\nu}$ selection on $q\bar{q}\gamma$ events reconstructed as we already explained.

Even if we could reject $q\bar{q}\gamma$ events without considering BGO inefficiencies it is more convenient to conceive a special rejection for this kind of events and we can do this starting from two sides. First, we rejected events when the missing energy was pointing within 20° from the edge of a dead BGO region (this margin was required by missing energy direction resolution), second we reject events when we found more than 2 GeV in that 60° cone defined in the upper section (EC60). This second selection criteria was justified observing that simulated photons

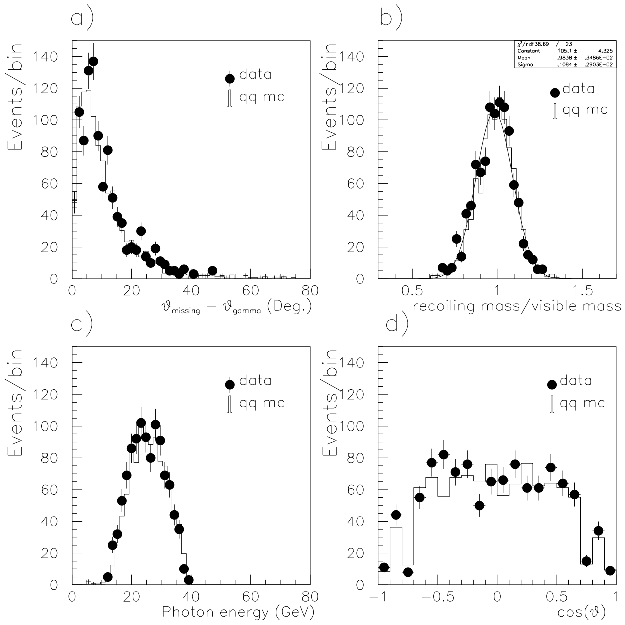

Figure 2: a) shows the angle between the photon and the missing energy direction obtained when ignoring the photon in the reconstruction; b) shows the difference between the mass recoiling to the photon and the mass computed from the hadronic system; c) and d) show the distributions of the energy and of the cos(polar angle) of the radiated photon.

of 25 GeV hitting dead BGO regions, in 60% of the cases, release more than 2 GeV just around the dead region which is always inside the 60° cone around the backward direction.
When we reject events whose missing energy is pointing to a dead BGO region, we suppress by a factor 10 this source of background but at the same time we loose an average of 7.8% relative efficiency for the Higgs. After this special rejection (cut on missing energy direction and on energy released around the backward direction) we know that we expect from this background, in 91÷94 data sample, 0.35 events.

3.2.2 Strategy for Final Selection

An important point in searches is to decide a priori the strategy of the selection. As important as that is to know the number of expected events from the background once we have applied our selection. In Higgs search it is hard to satisfy these requirements because of lack of Monte Carlo statistics.

To overcome this problem we have developed two methods aimed to define the selection and to know the number of expected events from the background, at the same time. These two methods substantially overlap in their phylosophy and in their procedure, they differ just in one point: one tries to understand quantitatively the correlations between variables used in the analysis while the other defines a sort of single global variable for the selection. Here we give a brief explanation of the procedure while a more precise treatment will follow in a dedicated paper.

The first method works as the following: given the normalization of our sample, of Monte

Carlo or data, the number of expected events with a certain set of cuts will be

$$N_{expected} = N_{sample} * \prod_{i=1}^{N_{cut}} (1 - F_{R_i}(1 - \sigma_i)) \tag{1}$$

where F_{R_i} is the rejection factor (between 0 and 1) for i-th cut and σ_i is the correlation factor (between 0 and 1) between i-th cut and all cuts previously applied. Rejection and correlation factors are calculated from the Monte Carlo. The problem when we are going to cut on the extreme tails of our distribution is that there is not just a simple correlation of our variables but also what we call "anticorrelation". This means that usually a single variable can not reject all the background events without rejecting at the same time all the Higgs sample. So for certain variables we should not multiply their rejection factor but we should add them as they were acting on independent samples. To try to estimate that "anticorrelation" we multiply $N_{expected}$ by an anticorrelation factor obtained from a fit of the quantity $N_{observed}/N_{expected}$ obtained from the Monte Carlo sample. But at that stage this procedure is equivalent to obtain the number of expected events from a fit of a single global variable. So we are getting to the second method which just does this kind of fit.

As we said, we have now to describe the part of the procedure common to both methods. All the cuts of the analysis are tightened at the same time, step by step. This means that we fix the number of tightening steps and for each step every cut is increased by a quantity equal to $(upper\ limit - lower\ limit)/N_{step}$, where lower and upper limit are the starting and ending values of a certain cut during the tightening procedure. It is clear that the relative importance as well as the effectiveness of each cut depend on the choice of the limits for the cut ranges. So to be independent on that choice the upper limit, for each cut, is obtained as

$$up.lim._{cut_i} = low.lim._{cut_i} + (U.L._{cut_i} - low.lim._{cut_i}) * X_{cut_i} \tag{2}$$

where X_{cut_i} is a random number uniformly distributed between 0 and 1, $U.L._{cut_i}$ is the maximum possible ending value of a certain cut during the tightening procedure, while the lower limit is defined by the preselection.

At each step we have a number of events passing the cuts and a function related to the cut iteration step is fit on them. Our choice for this function is a gaussian but we tested an exponential as well. This function is then used to predict the number of events that should pass a certain set of cut. To avoid the bias induced by the sample for which the function is fit, we compare the number of predicted events with the number of events that actually pass the cuts for an independent sample of Monte Carlo and we repeat the procedure randomly forming the two Monte Carlo samples, the one to be fit and the one to verify the prediction.

So to check the quality of the fit and that the function used is indeed correct, we filled a histogram with the number of events, which pass a given set of cuts, at an abscissa given by $x = (N_{step} - X_0)/\sigma$, where N_{step} is the tightening step of cuts from 1 to 100, X_0 is the mean and σ the standard deviation of the gaussian used for the fit. The histogram is filled for many random ranges and Monte Carlo samples if $\sigma > X_0$ and therefore we expect to observe a gaussian with mean 0 and $\sigma = 1$ for $x > 1$. Figure 3 shows such histograms for the Monte Carlo sample used for the fit a), for the test sample b), for the data c) and for the Monte Carlo test sample to which a 60 GeV Higgs signal has been added d). Clearly the test sample shows a wider distribution; this is due to the bias induced by the tail of the sample used for the fit. We can also observe that the behaviour of the data is very similar to the one of the Monte Carlo test sample. Finally we observe that if a 60 GeV Higgs boson existed we would have a great enhancement of the tail of the distribution.

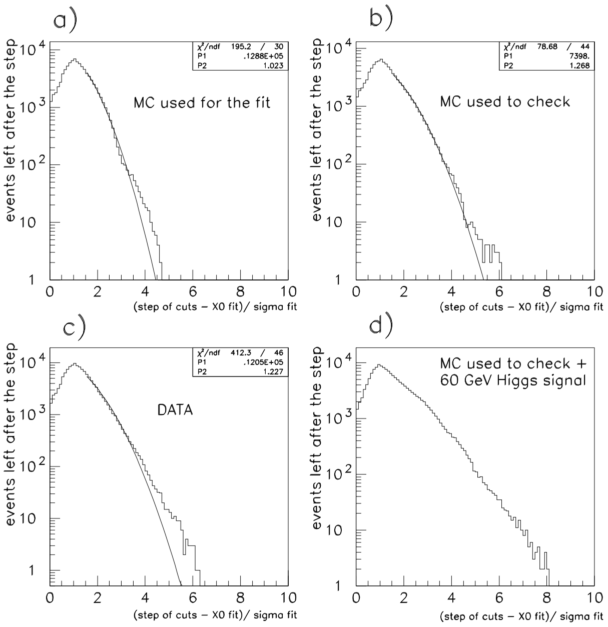

Figure 3: The distribution of the events which pass a certain cuts step, randomly iterated for many cut ranges and Monte carlo samples: a) for the fit Monte Carlo, b) for the check Monte Carlo, c) for all the data and d) for the Monte Carlo test sample to which a 60 GeV Higgs signal has been added. Events are normalized to the gaussian which results from the fit Monte Carlo, random step per random step.

From the comparison between these two histograms we estimate a correction factor of 1.3 to be used to broaden the standard deviation of the gaussian obtained from the fit in order to better estimate the number of expected events. At this point we fix the number of expected events from the background to 0.25 and we optimize the signal efficiency using the whole Monte Carlo background sample. The optimization is performed for a 60 GeV Higgs boson with the minimization program MINUIT.

Concluding these methods, which produce the same results, give the possibility to solve the two problems explained at the beginning of this section and they are not such dependent on the statistics of the Monte Carlo sample on which the procedure is performed. In addition to that, because with this procedure we reduce the selection to one equivalent variable, we could also decide to cut the last data event (without considering the efficiency loss) still maintaining a correct definition of the confidence level, provided that the variables involved in the procedure are chosen once for ever.

3.2.3 Selection Procedure

An initial selection, which has a very small effect on the Higgs signal, was made to reduce the size of data and Monte Carlo samples. First of all we require:

$$0.275 < E_{visible}/\sqrt{s} < 0.879$$

. We also require some quality cuts to reject badly reconstructed events:

- $E_{BGO} > 5$ GeV
- $E_{HCL}/E_{BGO} < 3$
- $DCA_{\mu} < 4$ m
- less than 3 muons per event

and to reject beam gas interactions $good\,tracks/total\,tracks > 0.2$, where for the so called good tracks we have some quality cuts on the number of hits in the TEC and on the $P_{\perp}$ of the track already shown in section 3.1 . As Higgs events have a lot of tracks and clusters we can easily reject $\tau^+\tau^-$ background with the following requirements:

- at least 6 charged good tracks per event
- at least 15 energy clusters per event

The selection that follows is aimed, with some simple cuts, to reject $e^+e^-q\bar{q}$ events

- energy in luminosity monitor less than 15 GeV
- transverse missing momentum$/E_{visible} > 0.13$
- transverse missing momentum > 7 GeV
- parallel missing momentum$/E_{visible} < 0.4$
- $E_{visible}/\sqrt{s} > 0.45$
- $\sin(\theta_{missing}) > 0.4$

- min $(E_{jet})/E_{visible} > 0.25$

After this preselection no $\tau^+\tau^-$ event and only 4 $e^+e^-q\bar{q}$ events are left in the Monte Carlo sample, corresponding to 2.2% of the total expected background. At this stage we have a good agreement between data and Monte Carlo for normalization and for all the variables.

Figure 4 shows data - Monte Carlo comparison after the preselection against $\tau^+\tau^-$ and $\gamma\gamma$ events for the transverse missing energy, for the acoplanarity, for the sum of the angles, in space, between three jets (SJET) and for the ratio between the sum of particle momenta transverse to the jet direction and the jet energy, for the narrow jet (NOVN).

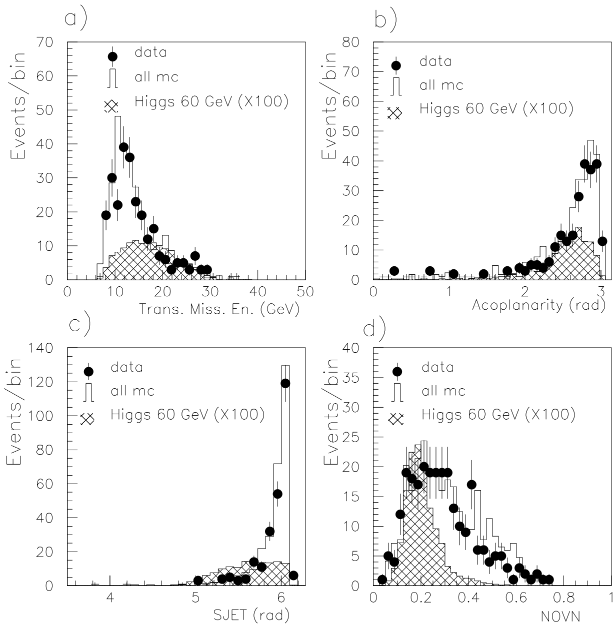

Figure 4: a) shows the transverse missing energy distribution; b) the acoplanarity distribution; c) the distribution of SJET (see text); d) the distribution of NOVN (see text).

After that we applied a further selection to reduce the Monte Carlo sample with variables that will be further tightened in the procedure described in previous section.

Finally from that procedure we get the value for the cuts when we expect 0.25 events from the background in 91÷94 data sample:

- acollinearity < 2.77 rad
- acoplanarity < 2.97 rad
- SJET < 5.86 rad
- NOVN < 0.494
- NOVB < 0.621
- EM25 < 0.74 GeV
- EMF25 < 7.83 GeV

- transverse missing energy   unchanged with respect to the preselection
- $\sin(\theta_{missing})$ unchanged with respect to the preselection
- $\sin(min(\theta_{jet})) > 0.4$

All the variables indicated in upper case were already defined in section 3.1 . Applying the final selection we do not observe any Higgs candidate in the data; while for the Monte Carlo samples just one $\tau^+\tau^- b\bar{b}$ event survives (corresponding to 0.02 $\tau^+\tau^- q\bar{q}$ events in our data sample) and a number of $\nu\bar{\nu}$q$\bar{\text{q}}$ equivalent to 0.01 events in our data.

Figure 5 shows the distribution of the events which pass a certain cuts step, for the fitted Monte Carlo and for all the data for the final choice of cuts ranges, obtained minimizing the average Poisson upper limit divided by the signal efficiency. The minimization gives a number of expected events equal to 0.25.

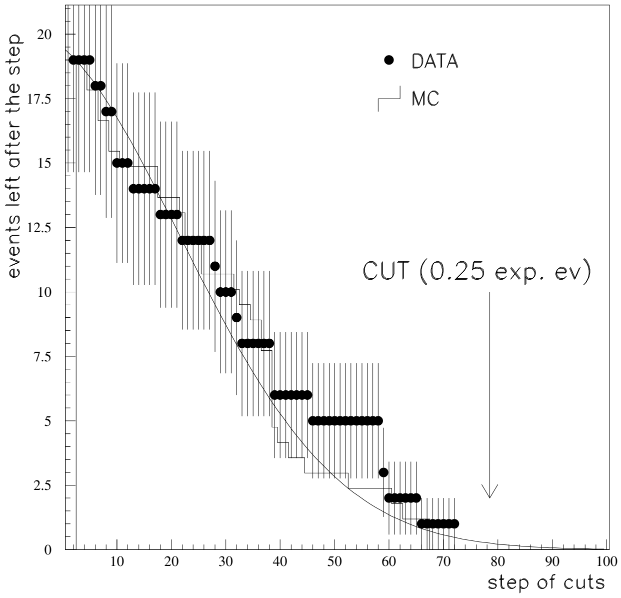

Figure 5: Final sequence of cuts, the curve indicates the gaussian fit to the Monte Carlo, the arrow the position of the final cuts.

The signal efficiencies for Higgs mass ranging from 50 GeV to 70 GeV are reported in Tab. 3.2.3 , while in figure 6 we have the signal efficiency as a function of the number of expected events from the background for $M_H = 60$ GeV.

3.2.4 Systematic Error Estimation

We have taken into account various sources of systematic error on the signal detection efficiency:

1. uncertainty on energy scale
2. uncertainty on subdetectors response
3. uncertainty on fragmentation model for the Higgs boson

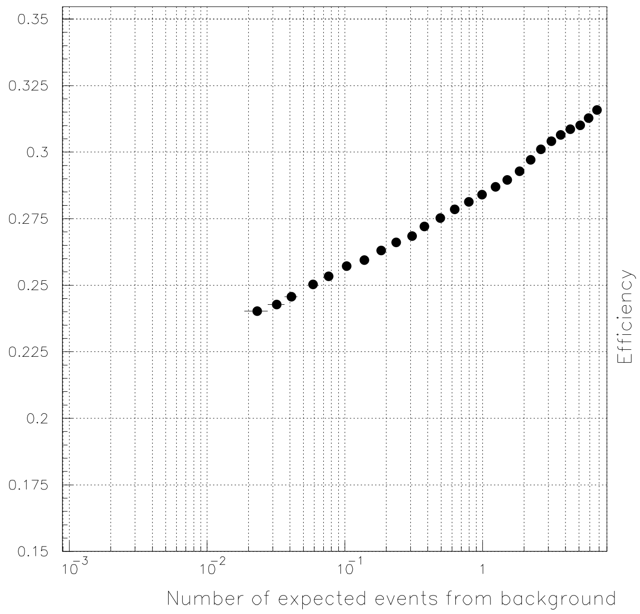

Figure 6: Signal efficiency versus number of background expected events for the final choice of cut ranges. A dot is produced for every cut step.

M_H(GeV)	Efficiency (%)
70	9.2
65	16.0
60	26.6
55	31.1
50	34.8

Table 1: Signal detection efficiency for different Higgs masses.

Source of systematics	ΔEffic./Effic. (%)
Calibrat. const. + Ener. scale	$0. \pm 0.5$
Angles	-0.7 ± 0.5
Tracks	negligible

Table 2: Systematic errors on signal detection efficiency.

4. TEC inefficiency
5. uncertainty on jet angular resolution.

To estimate the effect of the first source of systematic error we varied the global energy scale according to a normal distribution with $\sigma = 3\%$. This variation was derived by a comparison between JETSET and HERWIG calibration constants: actually exchanging each other these constants we observed a shift on mean visible energy of 3%.
For the estimation of the second source of systematic error the best way we found is to change independently each calibration constant, corresponding to a particular region of the detector, according to a normal distribution. The third source of systematic error is strictly related to the previous one for two reasons: first because variations concerning the fragmentation model involve different energy distributions and, as a consequence, a different relative importance of each region of the detector; second because the way we extract the variation for each calibration constant includes also the variation due to the fragmentation model. Actually each calibration constant has a σ equal to the difference between its value obtained with JETSET and with HERWIG, typically of the order of 5%.
TEC inefficiency was taken into account both for the cut on minimum number of tracks per event and for our energy counting algorithm which considers tracks momentum too. Single track inefficiency was derived both from a study of τ three prong inefficiency and from a comparison between data and Monte Carlo $q\bar{q}$. We found the same result of 2.7% of single track inefficiency. Finally we conclude that this source of systematic error is negligible for our analysis.
The effect of the fifth source of systematic error is evaluated smearing, according to a normal distribution, the θ and ϕ jet direction. The σ for these distributions are extracted in a very conservative way: actually from a comparison of data and Monte Carlo $q\bar{q}$ we observe that the function representing the angular resolution is a double gaussian (see figure 1), so we take the discrepancy relative to the broader gaussian, that is 0.7° for θ and 1.7° for ϕ.

Results, for all these effects, are shown in Tab. 2.

As total systematic error on signal detection efficiency we take the average shift plus one σ that is 1.3%.

Other sources of systematic errors on the number of expected Higgs events are the following:

- Theoretical uncertainty of less than 1% on the ratio between the Higgs boson production cross section and the $e^+e^- \rightarrow q\bar{q}$ cross section
- Experimental uncertainty of 1% on the corrected number of hadronic Z decays used for the normalization
- Theoretical uncertainty on the Higgs decay branching ratios which contributes with an error of 0.7% to the detection efficiency
- Error on the Higgs detection efficiency of 2.4% due to Monte Carlo statistics.

Combining these errors in quadrature with the systematic error on the efficiency we obtain a systematic uncertainty of 3.1%.

3.3 Mass Range 15 GeV $< M_H <$ 50 GeV

3.3.1 Introduction

The analysis in this mass region is performed exactly in the same way as in the high mass region. We use the same variables and the same strategy to set the final selection.

Some considerations on the signal and on the backgrounds should be done. Signal events, due to the large amount of missing energy, are very unbalanced and this feature allows a good separation with respect to hadronic decays of the Z . On the other hand two photon interactions with hadronic final states are rejected requiring large visible energy and large total transverse momentum.

3.3.2 Selection Procedure

We apply on MC and data sample the same preselection described in section 3.2.3 except a modification concerning the energy range required which is now:

$$0.1 < E_{visible}/\sqrt{s} < 0.879$$

Applying the same procedure as for the high mass we optimize the efficiency for $M_H =$ 30 GeV once we have fixed the number of expected events from the background. From this minimization we obtain the following values for the final selection:

- transverse missing momentum/$E_{visible} > 0.344$
- $E_{visible} > 53.8$ GeV
- transverse missing momentum > 9.14 GeV
- parallel missing momentum/$E_{visible} < 0.6$
- $\sin(\theta_{missing}) > 0.503$
- min $(\mathrm{E}_{jet})/E_{visible} > 0.25$
- acollinearity < 2.69 rad
- π-(min(sin(θ_{jet1}),sin(θ_{jet2}))*(π-acoplanarity)) < 2.67 rad
- SJET < 5.87 rad
- NOVB < 0.646
- $\min(\sin(\theta_{jet1}), \sin(\theta_{jet2})) > 0.4$

where all these variables are a subset of those for the high mass and they have already been defined in the previous sections.

3.3.3 Results

We did not find any candidate analyzing all the data set from 1991 to 1994. The expected background is 0.07 events from $q\bar{q}$ and two photon interactions and 0.03 events from $\tau^+\tau^-b\bar{b}$ and $\nu\bar{\nu}q\bar{q}$. The efficiencies for this selection are combined with those of high and low mass selections and are quoted in table 14 . The systematic errors for this selection are the same as those for high mass selection.

3.4 Mass Range 50 MeV$< M_H <$ 15 GeV

3.4.1 Introduction

The signature of the signal in this mass range is a monojet coming from the decay of the H^0 and absence of any activity in the region of the detector opposite to that monojet.

The main backgrounds are due to two photon interactions, where the detected particles have high total transverse momentum, and to $Z\rightarrow\tau^+\tau^-$ where a neutrino, coming from the decay of the τ, takes almost the whole available momentum.

In this mass range we should also consider trigger inefficiencies which are no longer negligible as it was for the high mass region.

3.4.2 Selection

The selection is based on some simple criteria: monojet requirements, antitag $\gamma\gamma$ interactions rejecting events with an electron tagged in the luminosity monitor or in the active lead ring and require a large total transverse momentum.

We apply some quality cuts to reject badly reconstructed events asking for the ratio between total visible energy (as defined in the high mass section) and total tracks momentum to be lower than 1.4, for every reconstructed muon to have a DCA lower than 50 cm, for some energy in the electromagnetic calorimeter. In addition to that when we have two prong events with muons we require at least 7 GeV measured in the muon chamber, this cut is necessary because of double counting of the momentum by TEC and muon chambers.

We select events with a visible energy below 60 GeV and if two jets are reconstructed we require the acoplanarity and the acollinearity of the two jets to be less than 2.8 rad. To exploit the monojet typology of the signal we ask one jet with at least two good tracks and at least 5 GeV of total energy while for the opposite hemisphere we ask a total energy lower than 3 GeV and the absence of any charged track.

We also ask that in a 25° h.o.a. sector, in the $R-\phi$ plane, opposite to the monojet direction there is no energy deposit. To reject $\tau^+\tau^-$background (three prong decay on one side and a very energetic neutrino on the other side) we ask the number of good tracks, in the monojet, to be different from three.

To reject events coming from $\gamma\gamma$ interactions we require less than 3 GeV deposited in the luminosity monitor and less than 10 MeV deposited in the ALR. These two cuts cost a relative loss of efficiency of 1.1% as we understood studying beam-gate events.

Finally we require a total transverse momentum greater than 7 GeV and the polar angle of the direction of the total momentum greater than 40°.

3.4.3 Efficiency Evaluation

Higgs boson search in this mass range implies a careful evaluation of signal efficiencies because some sources of efficiency loss are not reproduced, or badly reproduced, in the detector simulation. Actually we have to add some inefficiencies due to trigger, TEC, ALR and luminosity monitor.

To evaluate trigger efficiency for our signal we select some data, passing a selection similar to the one for the signal, triggered in a way independent with respect to the one which should select our signal and we look how many times the trigger of interest is on. Then we derive the trigger efficiency as a function of the calorimetric energy released in the detector and we weight our Monte Carlo events according to this efficiency. This efficiency loss, due to the trigger, is relevant for Higgs masses below 5 GeV .

As important as trigger efficiency is TEC efficiency because of the low multiplicity decays of low mass Higgs. Actually single track inefficiency is estimated in the Monte Carlo 3.4% while studying three prong decays of the τ we derive a probability of 6.1% to loose one track. So taking into account the two requirements related to charged multiplicity, for the monojet, we can loose efficiency when two prong or four prong events loose one track.

Efficiency correction factors, due to TEC inefficiencies, are shown in table 3 as a function of the Higgs mass. Signal efficiencies for the low mass search are shown in table 14 together

m_H (GeV)	0.1	0.3	0.5	2	5	9	15
$\Delta\varepsilon/\varepsilon$ (%)	-5.4	-5.4	-5.4	-5.4	-3.4	-2.8	-0.46

Table 3: Correction factor as a function of m_H.

with those for intermediate and high mass search.

3.4.4 Systematic Error Estimation

We have taken into account various sources of systematic error on the signal detection efficiency:

1. uncertainty on energy scale
2. uncertainty on subdetectors response
3. uncertainty on fragmentation model for the Higgs boson
4. uncertainty on jet angular resolution
5. TEC inefficiency
6. trigger inefficiency

The first four sources of systematic error have already been analized in the high mass section and we can do here exactly the same considerations. So we proceed in the same way as described there to evaluate the contributions of those sources of error. There is only one difference concerning the source number 2 for which now we take into account also a contribution coming from the uncertainty on the efficiency correction factor due to ALR and luminosity monitor.

We deeply treated the fifth source in previous section, here we can assume a systematic error due this source equal to half of the correction factor.

Source of systematics	ΔEffic./Effic. (%)
Calibrat. const. + Ener. scale	4.2
Jet Angles	negligible
Tracks	2.7
Trigger	11.6
ALR + Lumin.	0.5

Table 4: Systematic errors on signal detection efficiency for $M_H = 2$ GeV.

m_H (GeV)	0.1	0.3	0.5	2	5	9	15
$\Delta\varepsilon/\varepsilon$ (%)	15.4	15.4	15.4	15.4	10.3	9.0	8.6

Table 5: Total systematic errors as a function of M_H.

Also the last source has already been described in the previous section. To evaluate the related systematic error we multiply the trigger efficiency error, coming from the binomial distribution, for a certain energy range (1 GeV step) with the percentage of signal events in this energy range.

The results are shown in table 3.4.4 for a Higgs mass of 2 GeV . Besides these contributions we also considered an error due to Monte Carlo statistics equal to 8.6%, in the case of $M_H =$ 2 GeV , an error coming from the uncertainty on the number of hadronic events and finally the theoretical errors as already shown in the high mass section. Combining all these sources of error we get the total systematic uncertainty which is shown in table 3.4.4 for each mass point.

3.4.5 Results

Concerning the low mass search we have analized the data collected by L3 from 1992 to 1994, equivalent to 2.74 million of hadronic decays of the Z. In this mass range we did not include 1991 data because the ALR is present since 1992 and this detector is essential to tag $\gamma\gamma$ interactions and hence to reject this background.

We estimate the following background contributions: 1.0 ± 1.0 events from $\gamma\gamma \rightarrow \mathrm{e}^+\mathrm{e}^-\mu^+\mu^-$, 0.11 ± 0.03 events from $\nu\bar{\nu}f\bar{f}$. No events from all the other MC background samples analyzed (listed in section 2) pass our selection.

We have found one candidate in the data sample (from 1994), it has an invariant mass of 3.9 ± 2.4 GeV , a total transverse momentum of 7.06 GeV , a recoiling mass of 82.8 ± 3 GeV and it is consistent with the expected background.

4 $\mathrm{H}^0 e^+e^-$ Channel

4.1 Mass Range 30 GeV $< M_H <$ 70 GeV

The signature of this process is the presence of two energetic and well separated electrons coming from the virtual Z^* isolated from the H^0 decay products. The main sources of background are the four-fermion process $\mathrm{e}^+\mathrm{e}^- \rightarrow \mathrm{e}^+\mathrm{e}^-\mathrm{q}\bar{\mathrm{q}}$ and the double semileptonic decay $Z \rightarrow \mathrm{b}\bar{\mathrm{b}} \rightarrow \mathrm{e}^+\mathrm{e}^- X$.

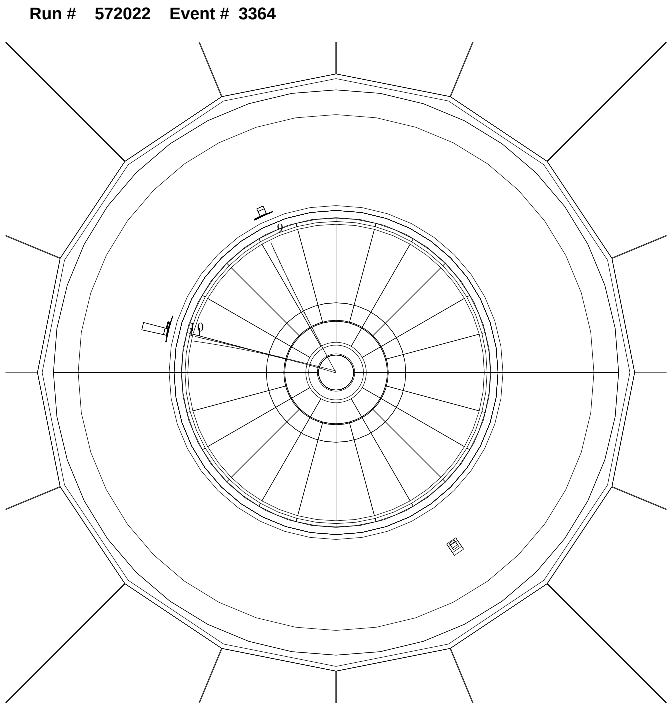

Figure 7: Low Higgs mass search candidate from 1994 data.

In our selection low multiplicity events, such as e^+e^- and $\tau^+\tau^-$ final states, are removed by requiring at least 16 clusters in the electromagnetic calorimeter.

To reduce the hadronic background in our sample we require that the two most energetic clusters have energies greater than 3 GeV and that the sum of their energies exceeds 15 GeV ; in addition the opening angle between these two clusters must be larger than 40°.

The identification of electromagnetic particles is mainly based on the energy deposition pattern in the electromagnetic calorimeter. We consider the ratio of the energy deposited in a 3×3 crystal array and the energy deposited in a 5×5 array both centred on the most energetic crystal in the cluster. After applying a position-dependent leakage correction to both measurements the distribution of this ratio is approximately gaussian, centered at 1.0 with a width of 1%. Electromagnetic candidates are identified by requiring that this ratio is less than 3σ away from the above mean value.

The isolation of the electron candidates is further ensured by imposing the following conditions: the additional energy deposited in the electromagnetic calorimeter between two cones of 5° and 15° half opening angle around the direction of the highest energy cluster must not exceed 1.9% of the cluster energy and the energy measured in the hadron calorimeter in the same cone must be less than 3 GeV ; the additional energy deposited in the electromagnetic calorimeter between two cones of 5° and 15° half opening angle around the second most energetic cluster must not exceed 1.9% of its energy.

To complete the identification of the electrons we consider all pairs out of the three most energetic electron candidates. The most energetic cluster in the pair is required to match in azimuthal angle with exactly one track and the second most energetic cluster with at least one track. For both clusters the matching has to be within a 4 σ cut where σ depends on the energies and on the polar angles of the clusters.

If the two most energetic electrons have an energy lower than 18 GeV , we consider the charges calculated with associated tracks in the TEC ($30^\circ < \theta < 150^\circ$). Their signs have to be opposite.

To identify the Higgs boson decay products we examine the non-electron jets in the event. Indicating with $P_\perp$ the transverse momentum of each electron with respect to the nearest jet, we require the sum of the two $P_\perp$ to be larger than 10 GeV , and each to be larger than 1 GeV .

To reject a background from the four fermion process we require that:

$$2M_{e^+e^-} + M_{\rm miss} > 80 \text{ GeV}$$

where $M_{e^+e^-}$ is the invariant mass of the electron pair and $M_{\rm miss}$ is the missing mass with respect to these electrons.

The selection efficiencies for the signal are shown in Table 7 for the 1991–1994 setups.

Two events passed the above selection criteria. The first one, with the missing mass to two electrons of 31.4 ± 1.5 GeV , is from the 1991 data sample; the second one, from the 1992 data sample, has the missing mass recoiling against the electron pair of 67.6 ± 0.7 GeV ; the main parameters of this event are summarized in Table 6 and the event is shown in Figure 8 .

	E (GeV)	θ (deg.)	ϕ (deg.)
jet$_1$	58.3 ± 8.9	152.3 ± 2.1	52.9 ± 2.1
jet$_2$	30.8 ± 5.5	36.6 ± 2.1	284.6 ± 2.1
e^+	4.8 ± 0.1	20.7 ± 0.2	127.7 ± 0.2
e^-	16.2 ± 0.2	63.4 ± 0.1	186.1 ± 0.3

Table 6: The energies (E), the polar angles with respect to the beam line (θ) and the azimuthal angles (ϕ) of the main constituents of the 1992 He^+e^- candidate are indicated. The main parameters of the event are: a visible energy of 109.0 ± 12.5 GeV, a missing mass recoiling against the final state electrons of 67.6 ± 0.7 GeV, an invariant mass of the electron-positron pair of 8.0 ± 0.3 GeV and a measured mass of the hadronic system of 82.2 ± 12.3 GeV.

Both observed events are consistent with the background process $e^+e^- \rightarrow e^+e^-q\bar{q}$ from which we expect 3.0$\pm$0.7 events for a recoil mass greater than 30 GeV (for a missing mass greater than 40 GeV we expect 2.6$\pm$0.7 four-fermion events). Less than 1 hadronic event with missing mass greater than 30 GeV is expected. The background from other processes is negligible. Figure 9 shows the missing mass distribution for expected background and data.

Higgs Mass (GeV)	30	40	50	60	65	70
$h^0e^+e^-$ channel (1991-94)	44.7	48.7	46.6	42.2	39.9	35.8

Table 7: Selection efficiencies (in %) for Higgs bosons with masses between 30 GeV and 70 GeV .

4.2 Mass Range 2 GeV $< M_H <$ 30 GeV

In this mass range the electrons coming from the Z^* are much more isolated, therefore we are left with only one important background: the four-fermion process $e^+e^- \rightarrow e^+e^-q\bar{q}$.

In order to remove low-multiplicity events, mainly e^+e^- and $\tau^+\tau^-$ pairs, we require at least 6 clusters in the BGO electromagnetic calorimeter and more than two tracks in the TEC, and

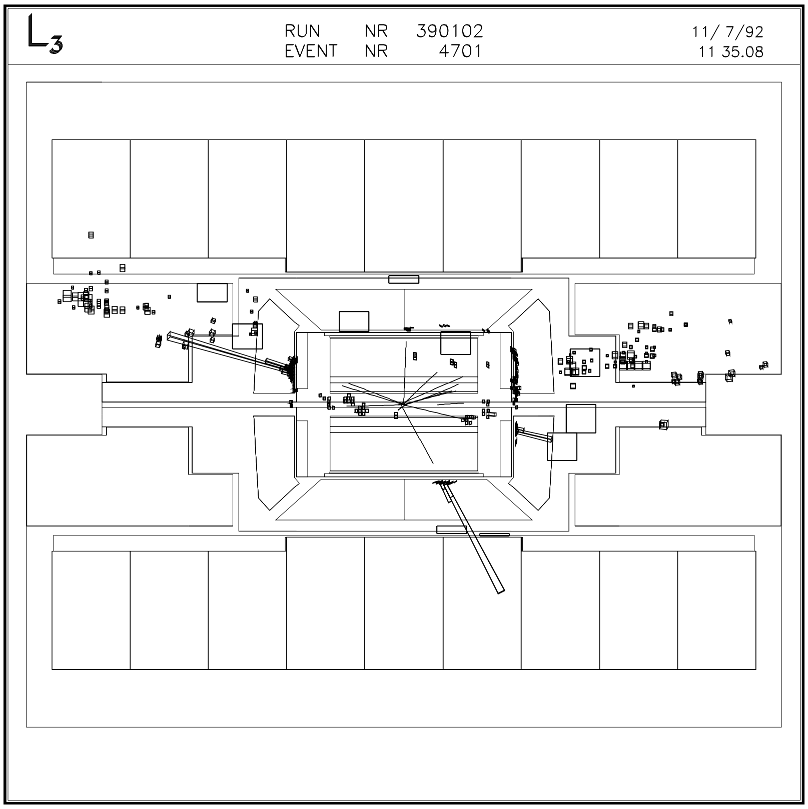

Figure 8: High mass Higgs candidate, found in 1992 data, from the $H^0 e^+ e^-$channel. The recoiling mass is equal to 67.6 ± 0.7 GeV.

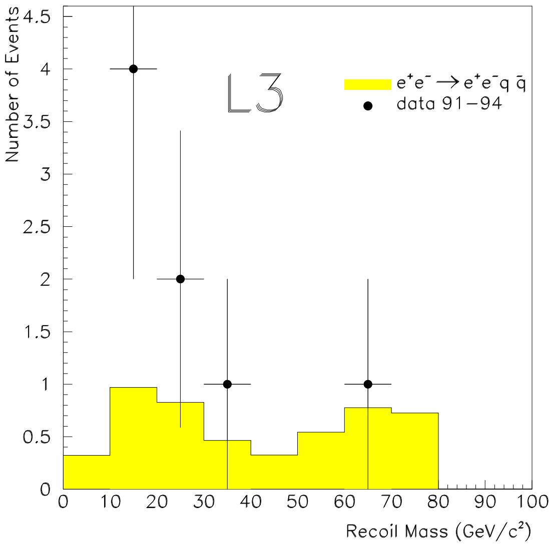

Figure 9: Missing Mass distribution for expected background and data, 91-94 setups

when the number of clusters in the BGO is lower than 11 we apply the additional following cuts :

The number of jets has to be greater than 2, the acoplanarity lower than 175°, and the third most energetic cluster must be lower than 3 GeV . Finally, to remove conversions we require the fourth cluster not to have two associated tracks.

To remove Bhabha events we select only events which have an acoplanarity lower than 179°.

To remove hadronic background, we select events with less than 50 clusters in the BGO and with the sum of the energy of the two most energetic electromagnetic clusters larger than 26 GeV . For the second most energetic cluster we require the ratio between the energies in cones of 15° half opening angle in electromagnetic and hadronic calorimeters not to be greater than 3.5.

The selection of isolated electromagnetic particles and their identification as electrons use the same criteria as in the high-mass range, with an isolation of 7% for both and one track for the second. TEC matching is also performed in θ, the polar angle, when this information from TEC z-wires or from Z-chamber is available, within a 4.5 σ cut in the sector ranging between 30° and 150°.

Then we examine the hadronic jets in the event. Defining P_t as the transverse momentum of an electron with respect to the nearest jet, we require the sum of the two P_t to be greater than 15 GeV and each P_t to be greater than 1 GeV. To remove four-fermion events the criteria used for the high-mass range is applied : $2M_{\mathrm{e^+e^-}} + M_{\mathrm{miss}} > 80$ GeV.

To take into account the gap between electromagnetic barrel and endcaps a fiducial cut is applied.

The Higgs boson selection efficiencies are shown in Table 8.

19 data events passed the above selection criteria. The missing mass distribution of these events is displayed on figure 10 and compared with the expected four-fermion background.

These events are consistent with backgrounds :

22.6 $\pm$ 1.5 expected events for four-fermion background and less than one expected event for $\tau^+\tau^-$ background.

Higgs Mass (GeV)	2	5	9	15	20	30
$h^0e^+e^-$ Channel	16.0	39.4	46.4	50.8	51.6	41.6

Table 8: Selection efficiencies (in %) for intermediate Higgs boson masses.

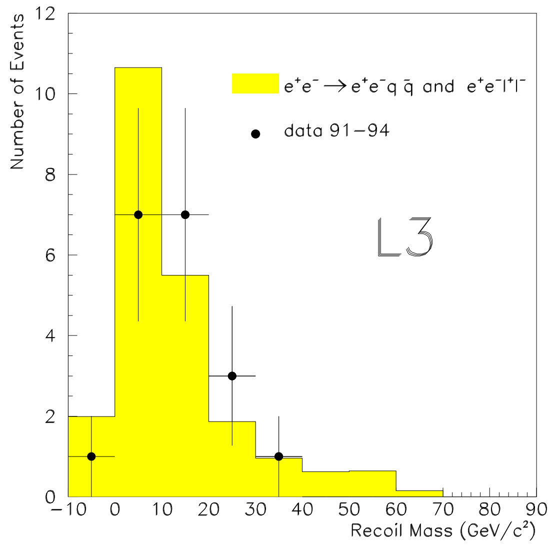

Figure 10: Missing Mass distribution for expected background and data, 91-94 setups

4.3 Mass Range $M_H < 4$ GeV

We search for a low-mass Higgs boson decaying into electrons, muons or hadrons. The main backgrounds with a similar signature are the four-fermion process and the radiative Bhabha with a photon converting in the beam pipe or in the material of the TEC chamber. For masses below 2 m_μ, due to the long life time of the Higgs boson, an event is expected to contain only two acoplanar electrons, coming from the Z^*, with no other detected particle balancing the missing momentum. The background for such events is mainly radiative Bhabha and $\tau^+\tau^-$ with the photon escaping detection.

In order to remove the high-multiplicity events (for example $e^+e^- \rightarrow q\bar{q}$) we keep only events with at most 6 tracks in TEC, 14 clusters in the BGO electromagnetic detector, and 5 clusters in the hadronic detector. We require at least two high-energy electromagnetic clusters in the BGO calorimeter matching one TEC track each, the second most energetic having an energy greater than 30 GeV . The identification of the pair of electrons, decaying from the Z^*, is performed exactly as in the high-mass range. The isolation of the electron candidates is achieved by imposing the following condition :

in a cone of 30° half opening angle around the direction of the electron candidates, there should be no non-electromagnetic bump with an energy greater than 3 GeV nor muon.

A matched TEC track is defined as a TEC track which is associated with an electromagnetic cluster. The missing energy vector to the two electrons is required to lie more than 15° from the beam. The cone of 30° half opening angle around the missing energy vector is named decay cone. The event is selected when one of the three following further set of requirements, corresponding to different possible final states with detected or undetected Higgs decay products, is verified :

- First set

  Two and only two matched TEC tracks, no hadronic activity in the angular acceptance not covered by the electromagnetic calorimeter, the acoplanarity angle of the two electrons must be larger than 0.05 radians (Bhabha rejection), no or more than two neutral electromagnetic clusters (Radiative Bhabha rejection).

- Second set

  At least one track in muon chambers.

- Third set

  The number of matched TEC tracks is less than 6 and more than 3, no electromagnetic cluster associated with two tracks (radiative Bhabha with γ conversion), in the decay cone the sum of the energy of hadronic and electromagnetic clusters has to be greater then 1 GeV , at least one hadronic or electromagnetic clusters and at least one matched TEC track must be inside this cone.

We have performed several Monte Carlo simulations with the Higgs boson decaying into pairs of e, μ, π, K at various masses in the range $M_h < 4$ GeV . The corresponding selection efficiencies are given in Table 9.

For the computation of the limit we must take into account also neutral decays of the Higgs for which the efficiencies are lower. So combining efficiencies for neutral and charged decays we take a conservative estimation of 9% for all channels.

Higgs Mass (GeV)	0.01	0.1	0.22	0.3	1.0	3.6
$h^0 \to e^+e^-$	8.2	7.4	-	-	13.6	-
$h^0 \to \mu^+\mu^-$	-	-	22.	-	28.	24.
$h^0 \to \pi^+\pi^-$	-	-	-	9.4	17.	15.
$h^0 \to K^+K^-$	-	-	-	-	13.	16.

Table 9: Selection efficiencies (in %) for light Higgs boson in the $h^0e^+e^-$ channel.

The number of events which satisfy the above selection is 35. This number has to be compared with the 26.9 events expected from backgrounds (5.7 Bhabha events and 21.2 four-fermions events). No event is expected from $\tau^+\tau^-$. A mass distribution of data events and expected background events coming mainly from four-fermion processes, is shown in figure 11. The mass of the decay products is calculated using the momenta given by the tracks, when the measured momentum is less than 5 GeV , and with the energies measured by the calorimeters in case of energetic tracks, of all particles other than the two electrons supposed coming from Z^*.

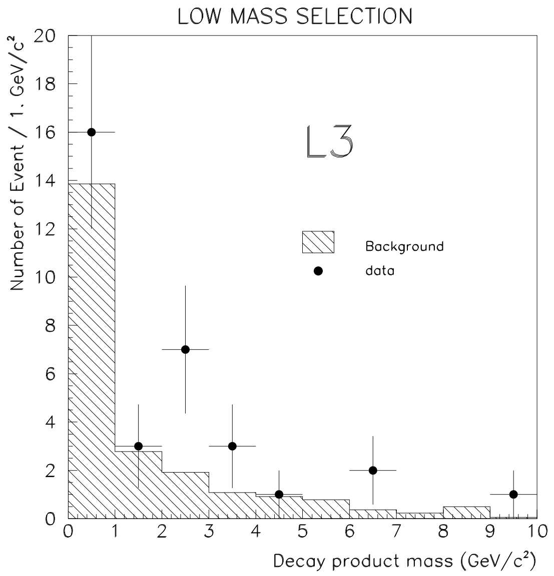

Figure 11: *Decay products mass distribution for data 91-94 and simulated background events.*

5 $H^0\mu^+\mu^-$ Channel

5.1 Mass Range 15 GeV $< M_H <$ 70 GeV

The main background processes, in this channel, are hadronic Z decays containing semileptonic μ decays and four fermion processes [11] $e^+e^- \to \mu^+\mu^- q\bar{q}$. Muons from hadronic Z decays are mostly included in the jet associated to the parton which has decayed semileptonically. Isolation criteria can reduce this background. The most dangerous contribution to the process $e^+e^- \to \mu^+\mu^- q\bar{q}$ comes from the diagram $e^+e^- \to Z \to q\bar{q}\gamma^* \to q\bar{q}\mu^+\mu^-$ where muons tend to have a low invariant mass. This background is definitely irreducible so one has to find a good compromise between contamination and efficiency.

Other processes containing two muons in the final state are $e^+e^- \to \mu^+\mu^-(n\gamma)$, $e^+e^- \to \mu^+\mu^- e^+e^-$, $e^+e^- \to \mu^+\mu^-\pi^+\pi^-$; these processes can be easily eliminated requiring a minimum number of tracks and a minimum number of calorimetric clusters.

The first requirement to the event is the presence of two muon tracks. In order to reduce the *punch-through* rate, a preselection cut of 2 GeV on the momentum of the muons is applied and a matching with the interaction vertex is required applying a cut on the extrapolated vertex (point of closest approach) of 3.5 standard deviations both in the z and the $r - \varphi$ projections.

In order to eliminate low charged multiplicity backgrounds, as $\mu^+\mu^-e^+e^-$ and $\mu^+\mu^-\pi^+\pi^-$, more than four tracks are required, and at least 8 calorimetric clusters.

A first reduction of both hadronic and 4 fermion background is obtained applying a cut on the thrust of the event.

The distribution of the thrust is shown in fig. 12. Data and Monte Carlo are normalized to the same number of events. A cut of 0.92 is applied.

Muons coming from the decay of the virtual Z present in the Higgs events tend to have high value of the momentum; on the contrary, muons from the γ^* of four fermion processes have preferably low momentum. A moderate cut ($p > 3.4$ GeV) on the minimum of the two muon momenta has been applied to slightly reduce the background without affecting too much signal

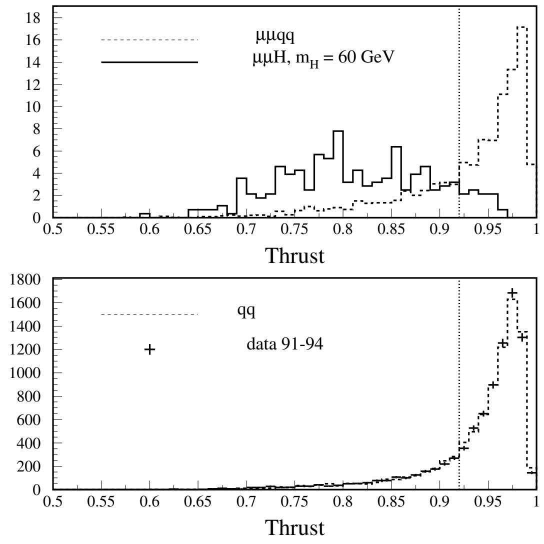

Figure 12: Thrust distribution for $\mu\mu H$ with m_H=60 GeV, $\mu\mu qq$ and qq Monte Carlo and data. The vertical line is the applied cut. The request for two muons and more than 4 tracks has been applied.

efficiency. Summing up the values of the two momenta (fig. 13), more sensitivity is obtained; a cut $p_1 + p_2 > 20$ GeV is applied.

The final selection concerns the definition of isolation variables for the muons.

For each muon we define:

$$\mathcal{D} = \frac{E_{jet} - p_\mu}{p_\mu} \tag{3}$$

where p_μ is the muon momentum and E_{jet} is the energy of the jet containing the muon. This variable is approximatively zero for isolated muons, and has large values for semileptonic muons, as shown in figure 14.

We consider the cone of 15° half opening angle with the axis on the direction of each μ; we compute $E^{15^\circ}_{bgo}$ as the electromagnetic energy in the cone; subtracting the deposit in the 3° half opening angle cone (fig. 15), which is essentially the muon M.I.P. energy deposition, we define:

$$\mathcal{E}_{bgo} = E^{15^\circ}_{bgo} - E^{3^\circ}_{bgo} \tag{4}$$

Semileptonic muons are generally contained in hadronic jets, with many particles surrounding it that give depositions in the calorimeters. These events have a large value of $E^{15^\circ}_{bgo}$, hence a large value of $\mathcal{E}_{bgo}$.

In a similar way we define:

$$\mathcal{E}_{hcl} = E^{30^\circ}_{hcl} - E^{3^\circ}_{hcl} \tag{5}$$

The three variables $\mathcal{D}$, $\mathcal{E}_{bgo}$ $\mathcal{E}_{hcl}$ have a good rejection power, expecially if the correlation between the two variables corresponding to the muons of the pair is taken into account. Then two-dimensional cuts have been applied and they have been established in order to reject all the events in the $q\bar{q}$ sample and reject as much as possible of the 4 fermion background. The

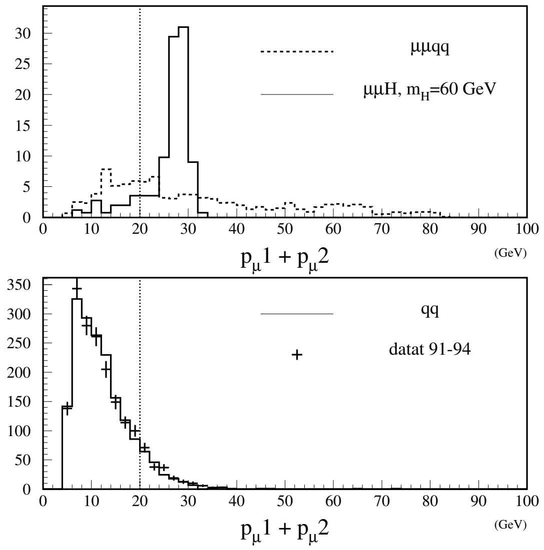

Figure 13: Sum of the two muon momenta. The vertical line is the applied cut. The request for two muons, more than 4 tracks and thrust cut have been applied.

analysis has been tuned on a Higgs mass $m_H = 60$ GeV which corresponds approximatively to the present limit. The cuts are the followings:

- $\mathcal{D}_{1,2} < 2.5, \quad \mathcal{D}_1 \times \mathcal{D}_2 < 0.25$;
- $\min(\mathcal{E}_{bgo}1, \mathcal{E}_{bgo}2) < 200$ MeV;
- $\mathcal{E}_{hcl}1, 2 < 4$ GeV, $\quad \mathcal{E}_{hcl}1 \times \mathcal{E}_{hcl}2 < 1$ GeV^2.

For the variables $\mathcal{D}$ and $\mathcal{E}_{hcl}$ hyperbolic cuts are more effective than straight cuts. Selection efficiencies are shown in table 10. of detector inefficiencies.

m_H (GeV)	15	20	30	40	50	55	60	65	70
ε (%)	25.7	29.5	37.0	37.1	36.1	33.7	32.3	26.2	3.3

Table 10: Efficiency as a function of m_H for $H^0\mu^+\mu^-$channel.

The background expected from $e^+e^- \to \mu^+\mu^- q\bar{q}$ is 1.8 ± 0.2 events; other sources of background give negligible contributions. The spectrum of the $\mu^+\mu^-$ recoil mass expected from the 4 fermion background is shown in fig. 16. No event survives in the data sample collected from 1991 to 1994.

5.2 Mass Range 2 GeV $< M_H <$ 15 GeV

In this mass region the signature of the signal is two energetic well separated muons recoiling against a hadronic system coming from the decay of the H^0. The main background is due to the four fermion processes [11] $e^+e^- \to \mu^+\mu^- q\bar{q}$. The selection is tuned to reduce this background

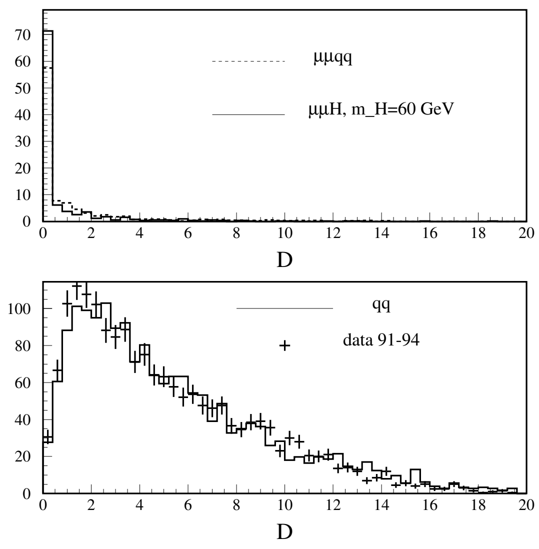

Figure 14: Spectrum of the variable $\mathcal{D}$.

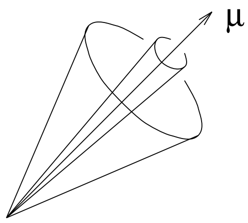

Figure 15: Cone definition.

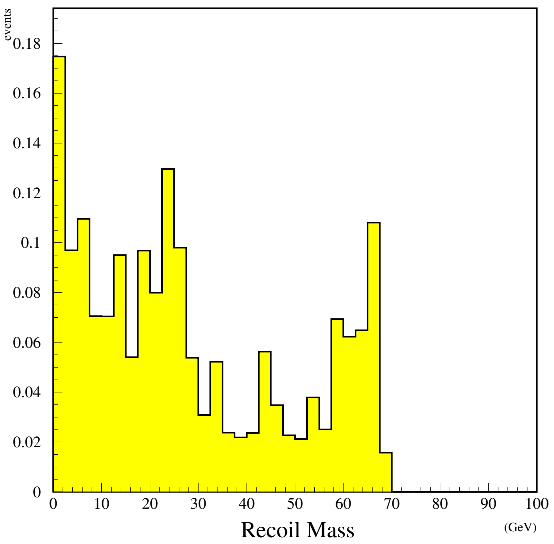

Figure 16: Spectrum of the $\mu^+\mu^-$ recoil mass of the expected 4 fermion background.

as much as possible and it is performed with the same variables as the high mass region but the values of the cuts are different due to the different kinematical region.

The first requirement to the event is the presence of two muon tracks. In order to reduce the *punch-through* rate, a preselection cut of 2 GeV on the momentum of the muons is applied and a matching with the interaction vertex is required applying a cut on the extrapolated vertex (point of closest approach) of 5.0 standard deviations both in the z and the $r - \varphi$ projections.

In order to eliminate very low charged multiplicity backgrounds more than 2 tracks are required, and at least 7 calorimetric clusters. At the same time we want to reduce high multiplicity hadronic systems, so less than 11 tracks are required.

Summing up the values of the two momenta, more sensitivity is obtained; a cut $p_1 + p_2 >$ 30 GeV is applied. But we want also to reduce four fermion background with the hadronic system coming from the radiated photon; we then require $\max(p_1, p_2) < 43$ GeV . We have also two requirements to define the kinematical region of interest: invariant mass of the muon system greater than 15 GeV and missing mass with respect to the muon system less than 25 GeV .

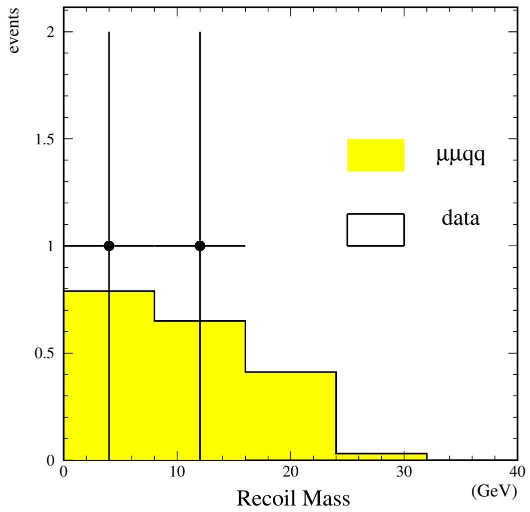

Figure 17: Spectrum of the $\mu^+\mu^-$ recoil mass of the expected 4 fermion background. The dots show the two candidates found in the data.

Finally we apply two cuts to require the isolation of the muon with respect to the hadronic system: $\min(\mathcal{D}_1, \mathcal{D}_2) < 0.3$, $\min(\mathcal{E}_{bgo}1, \mathcal{E}_{bgo}2) < 250$ MeV , where the variables $\mathcal{D}_{1,2}$ and $\mathcal{E}_{bgo}1, 2$ have already been defined in the high mass section.

Selection efficiencies are shown in table 11.

m_H (GeV)	2	5	9	15
ε (%)	8.5	21.7	27.6	17.1

Table 11: Efficiency as a function of m_H for $\mathrm{H}^0\mu^+\mu^-$channel.

The background expected from $e^+e^- \to \mu^+\mu^- q\bar{q}$ is 1.9 ± 0.2 events; other sources of background give negligible contributions. Two events were found in the data sample collected from 1991 to 1994. The first one from 1992 data with a missing mass with respect to the muons of 5.3 ± 1.0 GeV , the second one from 1993 data with a missing mass with respect to the muons of 9.6 ± 1.0 GeV . The spectrum of the $\mu^+\mu^-$ recoil mass expected from the 4 fermion background is shown in fig. 17 together with the two candidates.

6 Results

6.1 SM High Mass Higgs

As no data events survive the cuts in the neutrino channel and the candidate in the He^+e^- is far enough from the region of the limit, the 95% CL limit is set at a number of expected events of 3.

Figure 18 shows the number of Higgs events expected in the different channels, together with the 95% confidence level line and the Higgs mass limit at the 95% C.L.

We obtain a lower limit for the S.M. Higgs boson mass of:

$$M_H > 60.2 \text{ GeV at } 95\% \; C.L.$$

We report in Table 12 the efficiencies and in Table 13 the number of expected events, reduced by one standard deviation of the systematic error.

Higgs mass (GeV)	50	55	60	65	70
$\mathrm{H}^0\nu\bar{\nu}$ channel	34.8	31.1	26.6	16.0	9.2
$\mathrm{H}^0 e^+e^-$ channel	46.6	45.3	42.2	39.9	35.8
$\mathrm{H}^0\mu^+\mu^-$ channel	36.1	33.8	32.3	26.2	3.3

Table 12: Selection efficiencies (in %) for Higgs events in the different channels. The efficiencies are quoted for the process: $\mathrm{e^+e^-} \to Hl\bar{l} \to q\bar{q}l\bar{l}$.

Higgs mass (GeV)	50	55	60	65	70
$\mathrm{H}^0\nu\bar{\nu}$ channel	11.300	5.296	2.172	0.553	0.113
$\mathrm{H}^0 e^+e^-$ channel	2.498	1.274	0.570	0.228	0.072
$\mathrm{H}^0\mu^+\mu^-$ channel	1.876	0.920	0.422	0.145	0.006

Table 13: Number of expected Higgs events in the different channels for the high mass search, after subtracting one standard deviation of the systematic errors.

6.2 Neutral Two Doublet Model Higgs

For masses of the Higgs boson below 50 GeV we have used the combination in logical 'OR' of the analyses of the three mass ranges. The efficiencies are quoted in Table 14 for the $\mathrm{H}^0\nu\bar{\nu}$ channel. It is evident the efficiency drop for M_H below $2m_\mu$ due to the long life time of the Higgs boson.

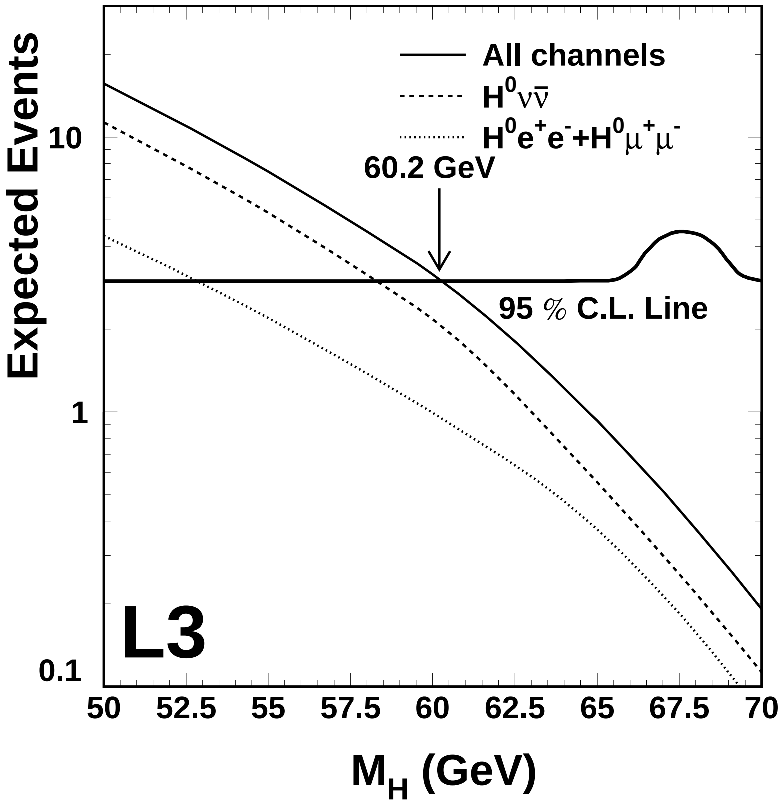

Figure 18: Number of Higgs events expected in the different channels. The 95% confidence level line is shown and the Higgs mass limit at the 95% C.L. is indicated.

Higgs mass (GeV)	0.05	0.1	0.3	0.5	2	5	9	15
$H^0\nu\bar{\nu}$ channel	0.	3.0	14.8	13.2	20.1	26.3	28.6	29.6
Higgs mass (GeV)	20	30	40	50	55	60	65	70
$H^0\nu\bar{\nu}$ channel	33.0	42.3	42.0	34.8	31.1	26.6	16.0	9.2

Table 14: Selection efficiencies (in %) for Higgs events in $H^0\nu\bar{\nu}$ channels.

M_A(GeV) | M_h(GeV)	3	12	24	40	48	58
1	24.1	-	16.0	-	-	-
3	-	-	-	-	13.2	-
11	-	-	-	-	40.9	-
12	-	-	-	37.1	-	24.7
20	-	-	-	-	-	8.8
22	-	-	-	-	19.8	-
24	-	-	-	-	-	4.0
4 ($A \rightarrow \tau^+\tau^-$)	-	27.2	19.8	-	-	-
11 ($A \rightarrow \tau^+\tau^-$)	-	-	-	-	8.0	-

Table 15: Signal detection efficiency, for the $h^0\nu\bar{\nu}$ channel, expressed in percent for different masses of h^0 and A^0 .

In this case the Higgs decays outside the TEC and the event does not have the charged tracks required by the selection.

In the framework of the two doublet model the decay of the h^0 into a pair of A^0 , when kinematically allowed, may be the dominant decay channel depending on the parameters α and β. We have then evaluated the efficiencies of our searches for this process for different mass points and different decay channels. They are shown in Tables 6.2,6.2,6.2.

6.2.1 Low Mass Results

We did not observe any evidence for the signal in the search for the SM Higgs boson in the three channels which have been studied. From this negative result limits can be obtained in the framework of non minimal Higgs models in which the bremsstrahlung Higgs production may be suppressed.

M_A(GeV) | M_h(GeV)	3	8	12	24	48
1	24.6	-	-	25.2	17.8
3	-	56.2	-	44.6	53.6
11	-	-	-	-	43.4
22	-	-	-	-	37.6
4 ($A \rightarrow \tau^+\tau^-$)	-	-	43.8	47.6	40.2

Table 16: Signal detection efficiency, for the $h^0e^+e^-$ channel, expressed in percent for different masses of h^0 and A^0 .

M_A(GeV) | M_h(GeV)	48
0.1	16.7
0.3	26.7
4	28.8
11	37.1
11 ($A \to \tau^+\tau^-$)	36.3

Table 17: Signal detection efficiency, for the $h^0\mu^+\mu^-$ channel, expressed in percent for different masses of h^0 and A^0.

Figure 19 shows the number of expected events, reduced by one standard deviation of the systematic error, and the 95% C.L. limit that we obtain on the ratio between the cross section of the bremsstrahlung production of the Higgs boson in the two doublet model and that of the SM Higgs boson, assuming that the non minimal Higgs boson has the same decay branching ratios.

The reduction of efficiency for the 1991 data due to the absence of the low mass analysis in the $H^0\nu\bar{\nu}$ channel has been taken into account.

6.2.2 Invisible Higgs Decays

If we consider the case of the production of a non minimal Higgs boson which decays into a final state which is invisible in the detector associated with a Z^* which decays into a pair of quarks, the signature is the same as that of the $H^0\nu\bar{\nu}$ channel. The previous analysis can therefore be directly applied and a limit can be derived on its branching ratio.

Table 18 reports the efficiencies for this search and Figure 20 shows the number of expected events, reduced by one standard deviation of the systematic error, and the 95% C.L. limit that we obtain on the ratio between the cross section of the bremsstrahlung production of the non minimal Higgs boson and that of the SM Higgs boson. The event which passes our selection is outside the mass range under consideration and therefore the 95% C.L. line is set at 3 events expected.

The reduction of efficiency for the 1991 data due to the absence of the low mass analysis has been taken into account.

Assuming that the cross section is the same as for the SM Higgs boson we obtain a lower limit for the mass of:

$$M_H > 66.7 \text{ GeV at } 95\% \ C.L.$$

Figure 20 shows the 95% C.L. limit that we obtain on the ratio between the cross section

Higgs mass (GeV)	0.1	5	10	20	30	40	50	60	70
Invisible Higgs channel	6.8	9.9	8.9	30.1	39.4	39.6	39.5	37.9	32.5

Table 18: Selection efficiencies (in %) for invisible Higgs decays.

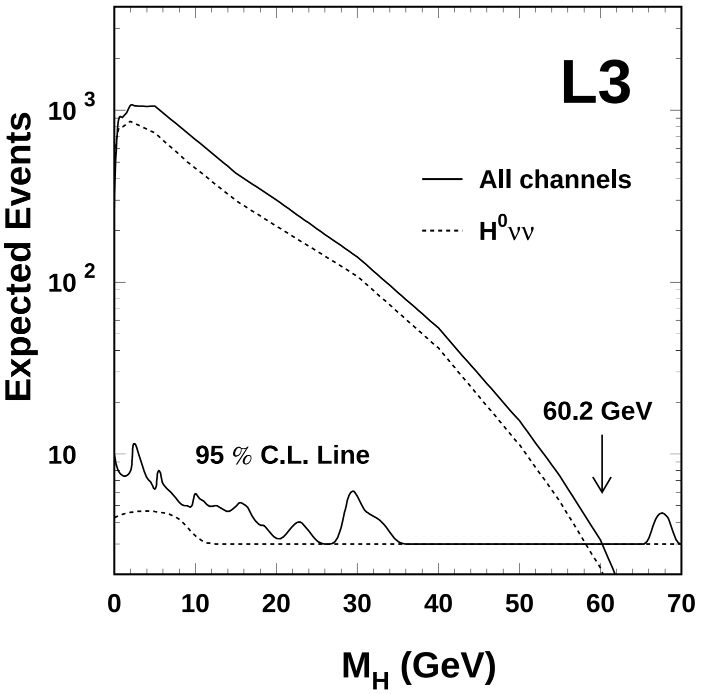

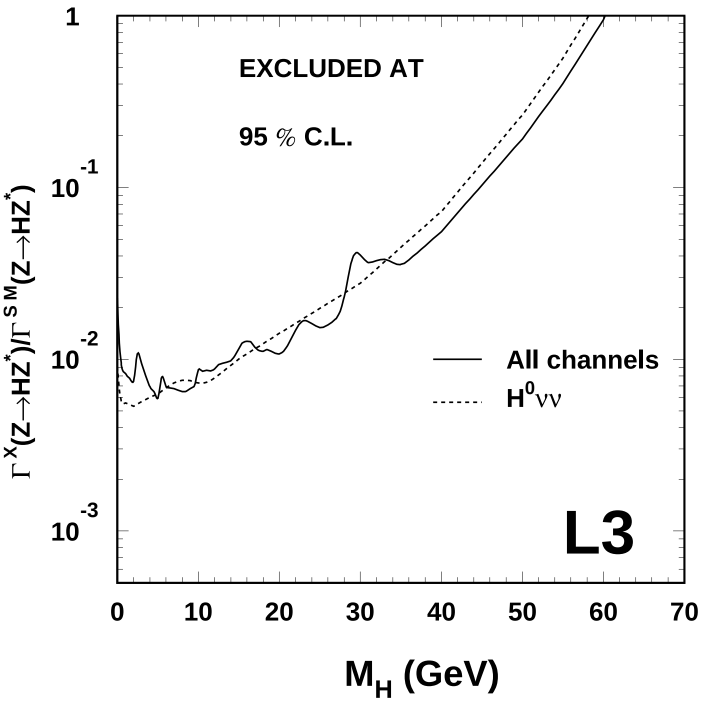

Figure 19: The upper figure shows the number of Higgs events expected in the different channels. The 95% confidence level line is shown and the Higgs mass limit at the 95% C.L. is indicated. The lower figure shows the ratio between the cross section of the bremsstrahlung production of the Higgs boson in the two doublet model and that of the SM Higgs boson.

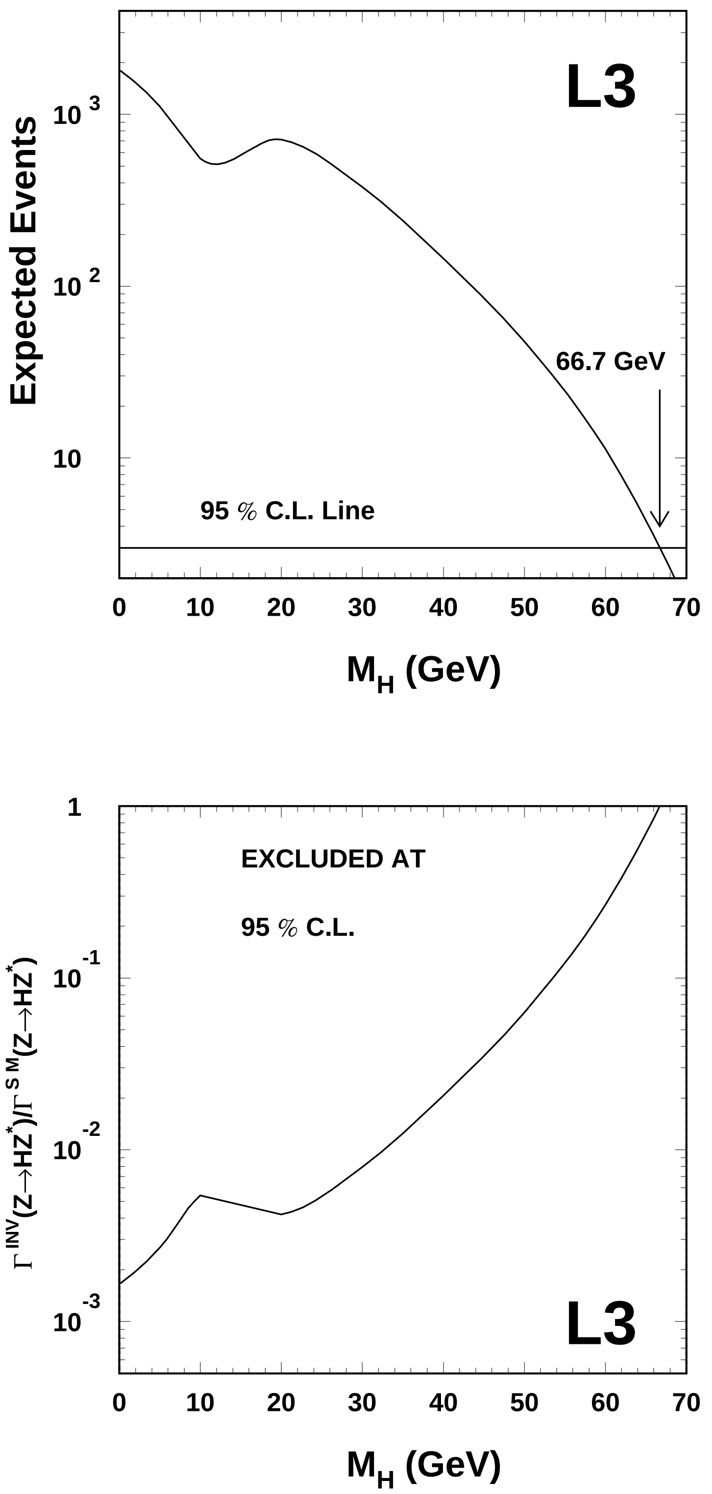

Figure 20: The upper figure shows the number of Higgs events expected for invisible Higgs decays. The 95% confidence level line is shown and the Higgs mass limit at the 95% C.L. is indicated. The lower figure shows the ratio between the cross section of the bremsstrahlung production of the invisible Higgs boson in the two doublet model and that of the SM Higgs boson.

7 Conclusions

We have searched for the neutral Standard Model Higgs boson production, in the process $e^+e^- \rightarrow Z^*\ H^0$, with data collected by L3 detector from 1991 to 1994, equivalent to about 3.05 M hadronic decays of the Z, at LEP e^+e^-collider. Three decay channels of the Z have been taken into account: $H^0e^+e^-$, $H^0\mu^+\mu^-$, $H^0\nu\bar{\nu}$. We did not find any evidence of the signal in all the mass range and we set a 95 % C.L. lower limit on the mass of the Standard Model Higgs boson of 60.2 GeV . These searches have also been interpreted in the framework of the general two doublet model and we set a limit on the ratio between the cross section of the bremsstrahlung production of a non minimal Higgs boson and that of the SM Higgs boson. Invisible decays of the Higgs boson have been considered and we derived a 95 % C.L. lower limit on the mass of the Higgs boson of 66.7 GeV for a production cross section equal to that of the Standard Model.

References

[1] S.L. Glashow, Nucl. Phys. **22** (1961) 579;
S. Weinberg, Phys. Rev. Lett. **19** (1967) 1264;
A. Salam, "Elementary Particle Theory", Ed. N. Svartholm, Stockholm, "Almquist and Wiksell" (1968), 367.

[2] P. W. Higgs, Phys. Lett. **12** (1964) 132, Phys. Rev. Lett. **13** (1964) 508 and Phys. Rev. **145** (1966) 1156;
F. Englert and R. Brout, Phys. Rev. Lett. **13** (1964) 321..

[3] B.L. Ioffe and V.A. Khoze, "What can be expected from experiments on colliding e^+e^- beams with $\approx$ 100 GeV ?", Sov. J. Part. Nucl. **9** (1978) 50;
J. D. Bjorken in "Proceedings of the 1976 SLAC Summer Institute on Particle Physics, Stanford", Ed. M. C. Zipf, (Stanford Linear Accel. Center, Stanford, 1976), SLAC-PUB-1866 (1977) 1;
J. Finjord, Phys.Scripta **21** (1980) 143..

[4] E. Gross, B. A. Kniehl and G. Wolf, Z. Phys. **C 63** (1994) 417.

[5] B. A. Kniehl, Phys. Lett. **B 282** (1992) 249.

[6] L3 Collab., B. Adeva *et al.*, Nucl. Inst. Meth. **A 289** (1990) 35.

[7] L3 Collab., O. Adriani *et al.*, Physics Reports **236** (1993) 1.

[8] T. Sjöstrand, Comp. Phys. Comm. **39** (1986) 347;
T. Sjöstrand and M. Bengtsson, Comp. Phys. Comm. **43** (1987) 367..

[9] G. Marchesini and B. Webber, Nucl. Phys. **B 310** (1988) 461;
G. Marchesini *et al.*, Comp. Phys. Comm. **67** (1992) 465..

[10] S. Jadach, B.F.L. Ward and Z. Wąs, Comp. Phys. Comm. **66** (1991) 276.

[11] J.Hilgart, R.Kleiss and F. Le Diberder, Comp. Phys. Comm. **73** (1993) 191.